Proceedings of ASME Turbo Expo 2023
Turbomachinery Technical Conference and Exposition
GT2023
June 26-30, 2023, Boston, Massachusetts

GT2023-101016

A METHOD OF PSEUDO-STEADY STATE CFD CALCULATION TO PREDICT TURBOMACHINE CHARACTERISTICS

Vlad Goldenberg
SoftInWay, Inc
Burlington, MA

Ben Conser
SoftInWay, Inc
Burlington, MA

Anna Vorobyova
SoftInWay Switzerland, GmbH
Zug, Switzerland

ABSTRACT

A method for performance-characteristic creation of a turbomachine has been developed to enable smooth characterization across various operating points without the need to simulate these points individually. The method itself involves the initial steady state CFD simulation of a turbomachinery flow path as is standard practice in the industry. This typically involves single blade row RANS analysis. The method involves adjusting the boundary condition(s) to sweep across a characteristic during simulation execution. The change in boundary conditions occurs at every iteration, however the change at each iteration is deliberately made sufficiently small so as not to significantly impact convergence characteristics such as equation residuals. Therefore, even though steady-state is never truly achieved during mapping of the characteristic, the rate of change is small enough that the method can be called a pseudo-steady state result.

In addition to generating a continuous characteristic, the method also enables the extraction and amplification of effects that are not otherwise easily predicted from steady-state CFD methods, and whose prediction and analysis using other methods, such as transient CFD computation, may be significantly more computationally costly. A specific example is the detection of stall/surge phenomena. A mathematical method has also been developed to evaluate stall behavior by applying a gaussian window filter on the convergence history and amplification of the resulting filtered convergence data. The method is most similar to experimental-based methods of stall and surge detection in that they rely on the detection of symptomatic phenomena such as vibration or acoustics rather than evaluation of underlying physics. Here, the detection of relatively small aggregate changes in steady-state simulation behavior is indicative of instability. The method is applied to three sample cases encompassing a broad sampling of turbomachinery: A multistage radial blower, a two-stage NASA transonic compressors, and an inducer pump.

Keywords: Compressor, CFD, Map, Stall, Pump, Cavitation

NOMENCLATURE

u_j	velocity in the j-coordinate
ρ	fluid density
x_j	j-coordinate in cartesian space
μ	viscosity
$p_{boundary}$	boundary pressure condition
p_{base}	starting/base pressure boundary
n_c	current iteration
$\dot{m}$	mass flow rate
δ_p	ramp rate for pressure
r_n	ramp rate for mass flow
σ	standard deviation (Guassian-filter)
I	Instability metric
n	iteration index
n_s	filtered iteration index
NPSH	Net positive suction head

1. INTRODUCTION

Prediction and evaluation of turbomachines' performance characteristics, such as map generation, range prediction, etc. is an important part turbomachinery lifecycle engineering that encompasses conceptual design, detailed design, validation, commissioning, in-service operational assessment, and rerates. Various tools have been developed that enable the deployment of the optimum resources vs. accuracy requirement to leverage the optimum combination. For example, during early conceptual design, absolute accuracy is rarely required. What is more important is to get an accurate tradeoff assessment that predicts qualitatively the effect of various design values on machine performance characteristics. More accurate and detailed 1D and 2D aerodynamic models are then needed to further develop the flowpath design. Many computer codes, encompassing in-house developments as well as major commercial software have been

developed to serve this need. AxSTREAM™ Flowpath is one example and was the tool used to develop two of the subject machines of this paper and a digital model of the third.

Computation fluid dynamics (CFD) is rarely used in this early stage of conceptual development. However, as the design matures and enters detailed design, a physics-based approach that CFD offers for evaluating the performance characteristics of machines independent of empirically-derived or semi-empirical performance models that may be dependent on traditional design space limits is sought. CFD has, in the last couple of decades, matured to a tool that is almost universally used and accepted to provide accurate information, within the limits of the modeling details users will incorporate into CFD models. Such CFD models can then be used to tune reduced order 1D/2D models (ROM) or can be used in standalone to provide information about in-service machines. The traditional practice is to perform steady-state Reynolds Averaged Navier Stokes (RANS) computation that uses semi-empirical turbulence models but otherwise is based on first-principles physics. Such calculations are typically performed at discrete operating points and have been validated to give results that are in good agreement with experimental data [1]. A potential disadvantage of using discrete operating points is that an indication of uncertainty in the results is not inherently given.

It is also desirable to be able to predict the operating range of turbomachines, especially compressors which have strict range limits set on the lower flow rate end by stall and surge phenomena. In the strictest definition, stall is a phenomenon that occurs inside the flow path when low fluid flow rate results in departure from the ideal alignment of fluid flow vector and blade orientation. Surge, on the other hand, is strictly-speaking a system phenomenon whose characteristics are determined by the interaction of the flowpath with the external operating curve of the connected system. While stall and surge are not the same phenomenon, they are indeed highly related, and the location on the operating map of a compressor where surge occurs is typically very near the stall inception. Fundamental background of the phenomenon can be found in the abundant literature, for example [2,3,4]. It is important to note here that a compressor can be partially stalled but not yet surging. This aspect will be briefly explored and revealed in the present work.

Various workers have developed methods to predict the location of stall on an operating map, characterize the resulting dynamics, describe the flow field, and developed novel methods to detect and analyze stall and surge phenomenon both numerically and experimentally. One of the principle basic definitions for the location of stall/surge is to define it where the speed line on the pressure vs. flow graph has a zero slope [5]. This is a useful and very practical definition from an engineering perspective. It must be noted, however, that some operation to the left of this point is possible if the system characteristic is sufficiently steep to stabilize the positive slope.

Righi, et. al. [6] modeled stall behavior in an axial compressor using an augmented and simplified CFD method. Vagani, et. al. [7] used transient CFD simulations, which are time consuming but most physically realistic with respect to the underlying phenomenon, which is truly transient in nature. The fundamental transient nature of stall and surge leads also to experimental methods of detection, as demonstrated by Munari et. al. [8].

The last of the aforementioned work and similar methods provides some inspiration for the current method. We hypothesized that the fundamental transient instabilities will also result in instabilities with the CFD, and that through parameter variation and intelligent post-processing, the phenomenological instabilities can be detected even when using steady-state RANS methods. Finally, it is also emphasized that the method demonstrated is useful beyond just steady state performance characterization and stall prediction. For example, cavitation phenomenon in pumps is fundamentally an unsteady process and results in degradation of performance of the pump [9]. In this work, it is demonstrated that the pseudo-steady state method can generate a cavitation characteristic curve which is able to clearly assess the net positive suction head required ($NPSH_R$) for the pump.

The method presented here involves the gradual variation of boundary conditions in the execution of a CFD simulation, followed by specific methodology of post-processing the resulting output parameters of the flow field, in some cases involving the use of data filtering techniques.

2. MATERIALS AND METHODS

2.1 General CFD Methods

In this work, computational fluid dynamics (CFD) was used as the primary analytical method of analysis. As usual, this involves the solution of the fundamental physical equations involving material mass, momentum, and energy conservation, commonly referred to as the Navier-Stokes equations. There are three momentum-pressure equations – one for each spatial coordinate, one mass conservation, and one energy conservation equation. The most relevant for solving the direct flow field are the momentum equations, expressed in the following equation in Einstein index notation.

$$\rho\frac{\partial \mathrm{u_j}}{\partial t}+\rho\left(u_i\frac{\partial u_j}{\partial x_i}\right)=-\frac{\partial p}{\partial x_j}+\frac{\partial}{\partial x_i}\left((\mu+\mu_t)\frac{\partial u_j}{\partial x_i}\right)+S_{r,j} \quad (1)$$

$$\begin{cases} i = 1,2,3 \\ j = 1,2,3 \end{cases}$$

$$\frac{\partial \rho}{\partial t}+\frac{\partial(\rho u_j)}{\partial x_i}=0 \quad (2)$$

In this work, we use a steady-state approach because we are interested in extracting the overall machine characteristics. Therefore, the first term in the above Eq. (1) is near-zero. Some solvers use a false-transient approach to the solution algorithm, so the time-dependent term may be used to update the flow field solution. Additionally, the viscosity term has been expanded into the intrinsic fluid viscosity and the turbulent viscosity that arises from the Reynolds-average stress. The turbulent viscosity must be solved using a turbulence model. In this work, the "workhorse" $k-\omega$ SST model is predominantly used due to its wide applicability to complex industrial flows [10,11].

For the two compressor sets simulated, the fluid was set to air using an ideal gas equation of state, which accurately represents real fluid properties when pressures are not very high and temperature not low, as is the present case. Full energy modeling was employed in these two sets of simulations. For the pump, the fluid was a two-phase mixture wherein each phase is modelled by constant-property fluid, which in this case is a reasonable model. In the pump simulation, the energy transfer is generally a minor contribution to the fluid dynamics, and so was not modelled. The interphase mass transfer was handled by the Schnerr-Sauer bubble growth/collapse cavitation model. The primary fluid properties used for the R245fa used in the pump simulations are documented in Table 1.

Table 1: Two phase fluid properties used for inducer pump simulation

Property	Value
Vapor Density	14.1 kg/m^3
Vapor Dynamic Viscosity	1.094×10^{-5} Pa-s
Liquid Density	1315 kg/m^3
Liquid Dynamic Viscosity	3.288×10^{-4} Pa-s
Liquid Saturation Pressure	198 kPa

A moving reference frame (MRF) model was used to model the blade motion. This is a well-validated method to model the steady-state behavior of turbomachinery that also enables modeling a single rotationally-periodic blade passage and thereby reduce computational expense. Mixing plane interfaces are applied, as necessary, between rotating and stationary domains or regions. Such an interface does not fully resolve the true physics of wake mixing interactions but is sufficiently accurate for a large collection of situations. Furthermore, it enables the use of single blade passages with pitch changes (differing blade numbers) between stationary and moving domains with relative ease. For the rest of the boundaries, periodic boundaries (enforcing exact replication of the flow field parameters on matched periodic boundaries) are used, while smooth non-slip walls which enforce zero velocity at the wall boundary are used at wall surfaces including the blades, hub, shroud, and other walls. Inlets are specified with a total pressure, wherein the velocity field is calculated by the results of the simulation.

The outlet boundary specification is dependent on the specific simulation. For the case of the four-stage centrifugal blower compressor and the pump, the total mass flow rate through the outlet is specified. The pressure is determined by the results of the simulation and the specific velocity profile is also calculated by the results only constrained to maintain the specified outlet boundary mass flow rate. For the four-stage centrifugal blower compressor case, a total pressure of 99.3 kPa and total temperature of 323.85 K are set as inlet boundary conditions. The base mass flow rate value $\dot{m}_{base}$ from Eq. (4) is set in the project and is taken into account with relative iterations substep (R) for achieving the current mass flow rate ($\dot{m}_{out}$). This mass flow rate value is used as outlet boundary condition. Connections between domains are implemented with a "Stage" mixing model with constant total pressure on each of the interface sides. A rotational periodicity interface model is used for all domains except the volute. Ideal Gas with standard settings is set as working fluid for simulation. For the case of the NASA two-stage axial compressor, the outlet boundary condition was specified as a static pressure. The outlet flow field and mass flow were determined by the simulation solution.

The important aspect of the method discussed in this work is that the CFD simulation should be performed in pseudo-steady state. This means that it is desired to obtain a steady solution as usual, however it is also desired to perform a near continuous sweep of one (or potentially several) variable so that a characteristic is generated. We therefore adjust a particular boundary condition of choice during the solver execution in such a way that the simulation remains in a converged state at each iteration. It is important that the simulation begins the ramp condition in a converged state, and this is practically accomplished by performing a typical fixed-boundary condition simulation and using the results as the initial seed condition, and incorporating an initial unramped period for several hundred iterations in the ramping function. The way to accomplish this, perhaps obvious by now, is to make the adjustment at each iteration sufficiently small. For the four-stage radial blower simulation, the outlet mass flow rate specification is varied by decreasing it from the design condition and lowering it until the simulation stability is untenable. For the two-stage axial compressor simulation, the parameter of variation is the outlet static pressure. It was started at some nominally small value and allowed to slowly increase until the simulation became unstable due to surge-like behavior. Finally, the parameter varied for the pump cavitation study was the inlet total pressure, which was started at a large value (800kPa) and decreased gradually until bubble formation caused instability in the simulation. The following equations describe the method of variation of the boundary conditions.

$$p_{boundary} = p_{base} + \delta_p n_c \quad (3)$$

$$\dot{m}_{out} = \dot{m}_{base} R_n \quad (4)$$

$$R_n = 1 - n_c r_n \quad (5)$$

Eq. (3) describes the formulation used for the NASA axial compressor and the inducer pump simulations for which a pressure sweep was used, while Eqs. (4) and (5) describe the formulation used for the radial blower simulations for which the mass flow boundary condition sweep was used.

Table 2: Sweep boundary parameter and rate specifications for each of the three subject cases

Subject Case	Sweep Boundary	Rate
4-stage radial blower	Outlet total mass flow rate	$1/r_n = 12000$
NASA 2-stage axial fan	Outlet static pressure	$\delta_p = 10\ [Pa]$
Inducer pump	Inlet total pressure	$\delta_p = -15\ [Pa]$

2.2 Subject Cases and Mesh Settings

For the present work, three subject machines were used that represent a diverse set of turbomachines for which this method is applicable and which demonstrate various aspects of its usefulness.

The first subject case is that of a 4-stage radial blower used for industrial applications to drive large quantities of pressurized air. This case was part of a design activity for a specific existing application and was the initial motivation for the development of this method. It is common practice during design analysis to quantify the low flow limit of stable operation of a compressor as the flow at which peak pressure rise (most often total-to-static) occurs [5]. For low speed and lightly loaded stages, there may be a moderately stable zone of operation to the left of the peak pressure rise before deep stall occurs, and it was desired to evaluate this region. The geometrical details and performance parameters of the machine are proprietary so are not disclosed here. However, a 3D view is shown in Figure 1.

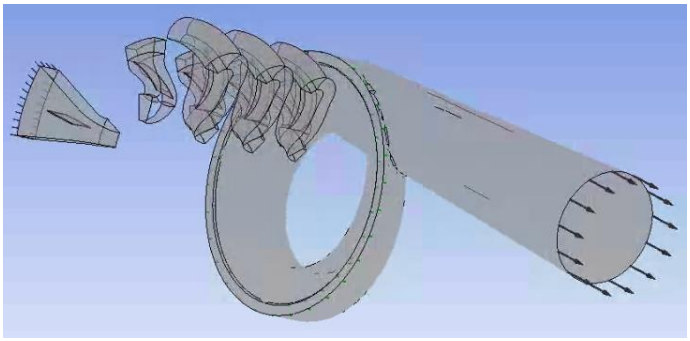

Figure 1: Computational domain for the 4-stage radial blower

The second subject case is a NASA transonic 2-stage axial compressor, a machine similar to the initial stages of many aero engine low pressure compressors. This case was selected because the geometry and experimental performance data are both available in the open literature [12], and therefore can serve to benchmark the absolute accuracy of the method. It is also significantly different from the previous case, and therefore lends some evidence that the method is generally applicable. The meridional profile and computational domain are shown in Figure 2.

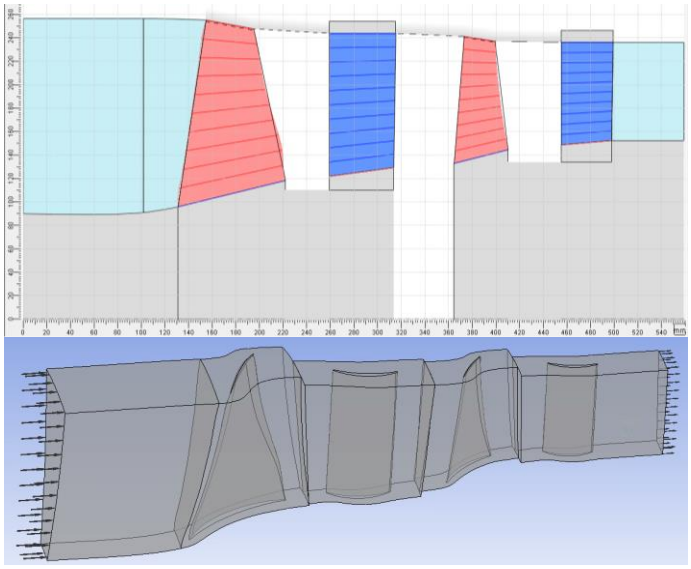

Figure 2: Meridional profile (top) and computational domain (bottom) for the two-stage axial compressor simulation

The design point performance of the 2-stage compressor is provided in Table 3.

Table 3: Design conditions of 2-stage compressor

Operating Parameter	Value
Working Fluid	Air
Total Inlet Temperature	15 °C
Total Inlet Pressure	101.325 kPa
Total Pressure Ratio	2.399
Mass Flow Rate	33.248 kg/s
Rotational Speed (nominal)	16042.8 rpm

The final subject case upon which the present method was applied is a small inducer pump. Such pumps are primarily axial flow with a diameter change between inlet and outlet and are exceptionally resistant to pumping liquid close to the vapor region and avoiding the ill effects of cavitation. The specific machine investigated here was designed to pump R245fa. The meridional profile and computational domain of this pump is shown in Figure 3.

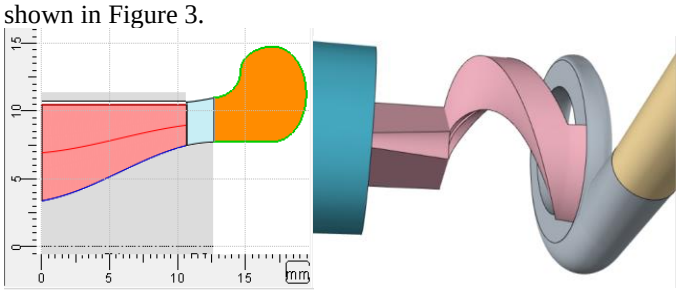

Figure 3: Design meridional profile for inducer pump and associated computational domain

It was desired to evaluate its cavitation characteristic at the design point. Therefore, the nature of simulation required is two-phase flow with interphase mass transfer, thus showing another unique application to this general method.

The total computational grid size for each subject machine is shown in Table 4.

Table 4: Computational grid summary and commercial solver used for each subject case

Subject Case	Number of Elements	Mesh Type	Solver
4-stage radial blower	~ 2.5×10^6	Hexahedra	Ansys CFX
NASA 2-stage axial fan	~ 4.9×10^6	Hexahedra	Ansys CFX
Inducer pump	~ 6.6×10^6	Polyhedra	Star-CCM+

Representative screenshots of the computational grids are shown in Figure 4, Figure 5, and Figure 6, respectively. In all simulations, care was taken to refine the grid near walls, as well as in tip gaps, as applicable. The mesh densities were primarily driven by the authors' experience in simulating a wide collection of turbomachinery using steady-state RANS on various solvers.

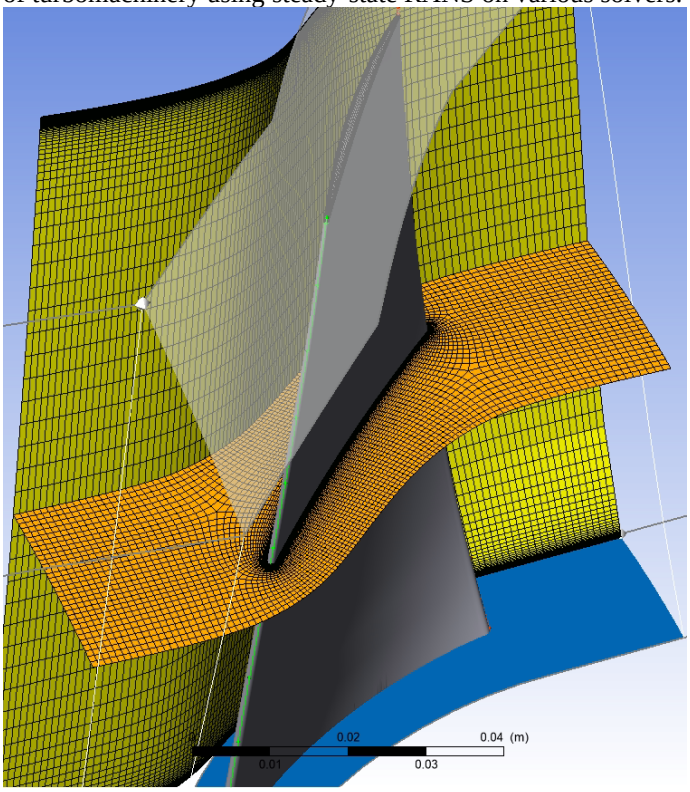

Figure 4: Representative structured mesh used to perform CFD simulations for the case of the NASA 2-stage compressor

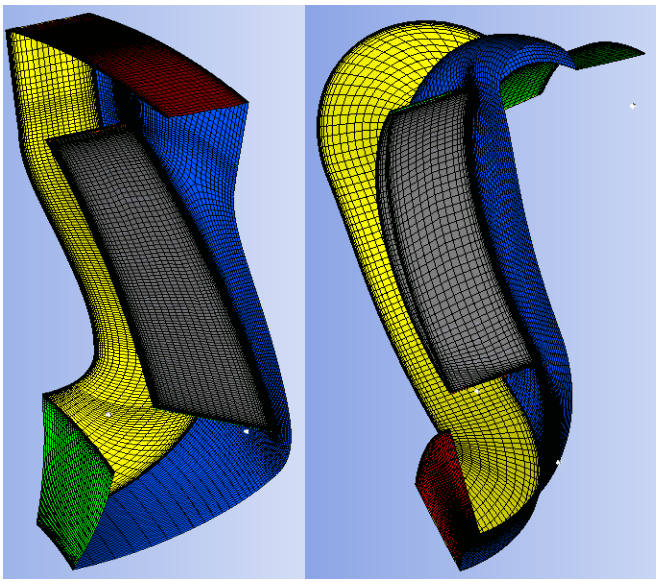

Figure 5: Representative structured mesh used to perform CFD simulations for the four-stage centrifugal blower compressor case (mesh for the impeller; mesh for the deswirler)

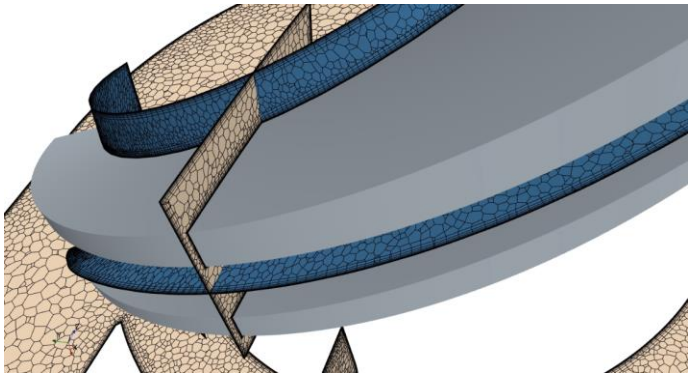

Figure 6: Representative mesh used to perform CFD simulations for the case of the inducer pump

2.3 Gaussian Filtering

It is necessary to apply a type of rolling-average filter to certain subsets of the simulation data. The precise algorithm to use and when the filter is applied depends on the type of data – whether it is residual values that are being analyzed, the physical imbalances, or the integral physical performance parameters, and will be discussed later. Each one will typically need the filter applied to enable most effective use of the data.

The selected filter is a Gaussian filter, selected because of its optimality with respect to filtering numerical noise with minimal use of iteration (pseudo-time) data. The equation for the Gaussian weighting function is shown in equation (6)

$$g(n, n_s) = \frac{1}{\sqrt{2\pi}\,\sigma} e^{-\frac{(n-n_s)^2}{2\sigma^2}} \quad (6)$$

Where σ is the standard deviation, a measure of the width of the Gaussian function that is familiar from standard statistical analysis techniques, n is the iteration index, and n_s is the sample

central iteration index upon which the Gaussian weight function is centered. Figure 7 shows an example of several Gaussian weighting functions. The gray and blue curves each have a $\sigma = 10$ value while the orange curve has a value of 5. The n_s values of the orange and blue curves are both 50, while that of the gray curve is 0.

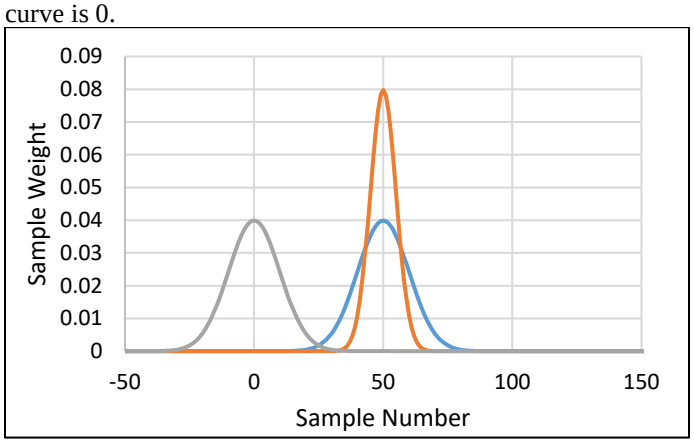

Figure 7: Display of several Gaussian filtering weight functions. $\sigma = 5, 10$ *and* $n_s = 0, 50$.

The evaluation of the Gaussian filtered data is done using equation (7) shown below.

$$f_g(n_s) = \sum_{n=n_s-k}^{n=n_s+k} g(n, n_s) f_0(n) \qquad (7)$$

Where $f_0(n)$ is the underlying CFD solution data at the nth iteration. It is necessary to limit the number of samples used because the data is finite, so it is somewhat arbitrarily chosen to set $2k = 10\sigma$. Thus, the number of samples used encompasses 10 standard deviations of the Gaussian, which results in less than 10^{-6} error, and for present purposes requires no further corrections to be made. Therefore, the choice to apply the filter to 10 times the standard deviation is a compromise between accuracy and data use, as the tail ends of the simulation data are not able to be filtered. It is important to emphasize here that $f_o(n)$ can be any iteration-indexed data from the simulation, whether it is integral performance data such as mass-flow-averaged parameters, or field data at specific locations, residuals, imbalances, or anything else.

As is clear from the previous equation, after performing filtering of any iteration-indexed data, the result is another set of iteration-indexed data that is only reduced in length by 2k (10 times the standard deviation, in the present work) but is otherwise able to be used or manipulated as the underlying data. The significant advantage of doing this is that inherent instabilities that exist in the simulation are smoothed and further it is possible to extract the magnitude of the instabilities for assessing stall and surge phenomena, for example. To understand clearly the reduction in iterations for a filtered data set, suppose there is a raw data set of 1000 iterations to which is applied a 2k value of 100. The resulting filtered data set is therefore 900 iterations in length, covering iterations 50 through 950, because the filter function is not defined on iterations 1-49 and 951-1000 as there is not sufficient data on the tail ends. The tail ends are essentially sacrificed and this is typically not an issue as the filter length should be significantly smaller than the length of the data set.

The filtering is first demonstrated on a contrived data set consisting of constant and linear data with a random error signal superimposed (Figure 8) and a step function signal with and without an error superimposed (Figure 9). Application of a Gaussian filter on either a perfect constant or linear data set trivially reproduces the original data, which is one of the reasons this filter was selected. However, if the underlying data also contains noise (due either to numerical effects of the simulation solver or physical effects such as the inherent time-invariant nature of a fluid flow), as simulated by a peak-to-peak unity random error in Figure 8, it is seen that the Gaussian filter removes the majority of the error and the underlying data is almost perfectly reconstructed.

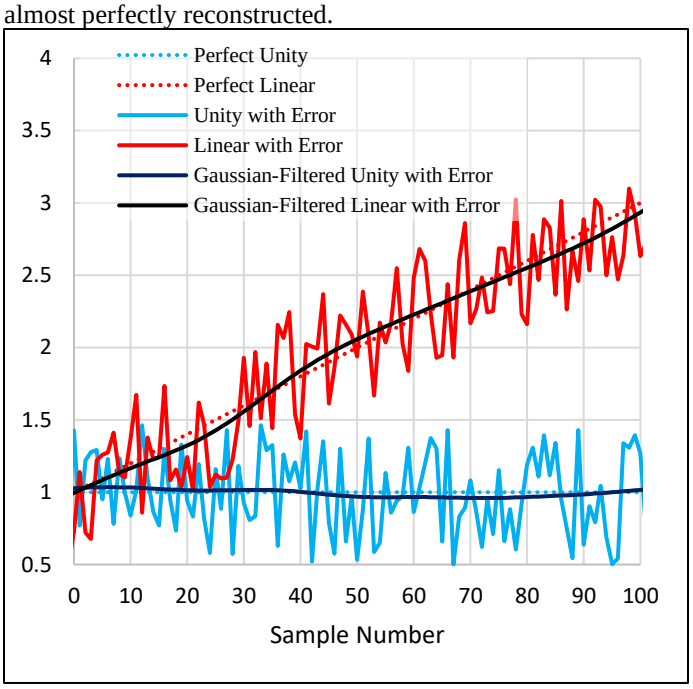

Figure 8: Application of a Gaussian filter of $\sigma = 10, k = 50$ *on constant (unity) and linear data with error.*

Looking at the simulated step function data of Figure 9, it is seen that even for perfect step function, the Gaussian-filtered result filters the transition, as is intended for near-steady state data where step transitions are not to be expected. Superimposing the simulated errors over the step function and applying the filter shows that the error filtered function follows the "perfect" step filter very closely, and both in fact get within the error magnitude within a standard deviation.

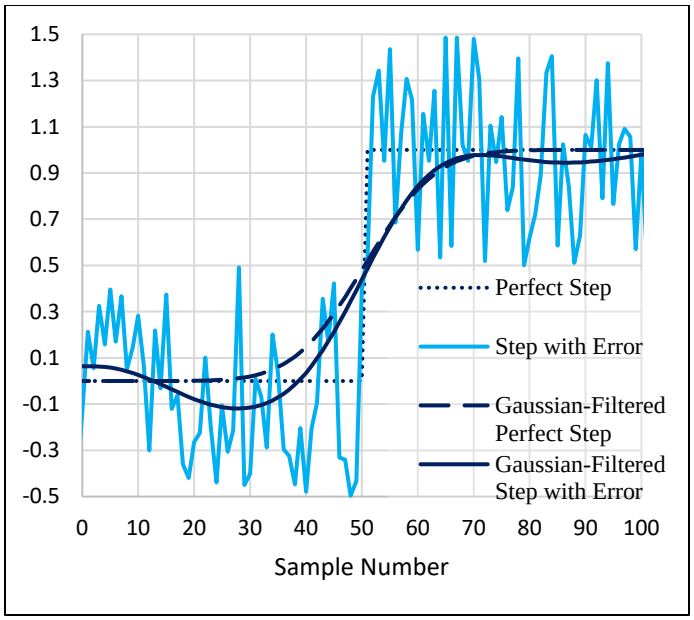

Figure 9: Application of a Gaussian filter of $\sigma = 10, k = 50$ on a perfect step function and a step function with random error.

Not all resulting data from the CFD simulations necessarily should be filtered. It will be seen that the characteristic developed in the pump simulation for the cavitation characteristic is sufficiently smooth without the need to perform the filtering. However, the method shown in this paper is especially useful in deriving characteristic behavior of turbomachinery near unstable regions such as choke or surge without knowing the operating values where these occur a-priori. For such simulations, where fundamental time-instability of the solution results in fluctuation of physical and numerical parameters, the Gaussian filtering method is particularly useful.

2.4 Stall/Surge Analysis

One final point needs to be discussed about application of the filtering and analysis. In addition to the goal of developing a turbomachine characteristic across an operating range, a central goal (and in fact motivation for development of this method) is to characterize the location and severity of stall and surge. There are a number of useful parameters that are generated in the course of the solution of most commercial CFD solvers. Here they are characterized into three classes:

- Residual metrics – numerical stability

It is common to characterize solution numerical convergence as a root-mean-square (RMS) or maximum value of the equation residuals for each element, and for each specific equation.

- Physical imbalances

These parameters are an indication of the physical soundness of the solution with regard to preserving the physical conservations laws (mass, momentum, energy) for domains or regions in the simulation. Some solvers (Ansys CFX, for example) include such parameters as default metrics to use for convergence evaluation and other use. Others may require users to write functions dependent on field variables. These should be below 0.01 relative and typically much less to consider a particular iteration to be valid.

- Physical parameters – derived from field functions

These are the resulting parameters, such as the mass flow rate at a boundary, the mass flow averaged total enthalpy, the isentropic efficiency, or multitudes of other parameters of interest.

For the purpose of developing a subjective metric of stability near stall, we take several metrics that are indicative of instability and make a product that effectively amplifies the instabilities. The above three classes of parameters are used in slightly different formulation with the product.

The first, the metric of equation residuals, is not actually the most important, or in fact even not a necessary one. It was, however, included in the final instability metric of the NASA 2-stage compressor. The equation residuals are generally a representation of the numerical stability, but not necessarily the physical stability of the simulation. It is most appropriate to take the product of the normalized RMS residuals directly before applying a filter because the residuals are the direct result of discretized equation imbalances in individual computation volumes. Thus

$$I_R(n) = \tilde{G}\left(\prod_i f_{R,i}(n)\right) \tag{8}$$

Where I_R is the instability metric associated with residuals, $f_{R,i}$ simply denotes the iteration-sampled residual data, with the subscript "i" referring to each of several equation RMS residuals that may be associated with a particular subdomain or the entire domain of the simulation, and the $\tilde{G}$ operator referring to the Gaussian filtering operation of equation (7). It is important to note that filtering only smooths the resulting metric and is not strictly necessary.

The second and third class of parameters are somewhat similar in that they are based on physical calculations from the flow field values. The key aspect is that the imbalances are near zero, and are indeed desired to go as close to zero as possible, while the physical parameters can be any value. Analogous to equation (8) above, an instability metric can be derived by taking the product of the imbalances. It is not necessary to perform any further filtering, however such filtering may provide a more objective graph. Alternatively, it is reasonable to perform filtering on the underlying data first before taking the product to amplify non-zero values, per the following equation.

$$I_B(n) = \prod_i \tilde{G}\left(f_{B,i}(n)\right) \tag{9}$$

This is quite justified because when the CFD simulation is being performed at steady-state or pseudo-steady state conditions as stipulated in this work, and is properly constrained, the imbalances are very small values and fluctuate about zero. Thus, the last method amplifies aggregate imbalances. This should be used with caution when applied with detecting surge-related instability while using pressure boundary conditions at both inlet and outlet, as the operation of the machine is highly sensitive to pressure near stall and surge. This will be further discussed in the results.

Finally, variation of the physical parameters of interest is also an indicator of instability. For this metric, it is necessary to take a measure of the fluctuation in the variable. An easy way to do this is to take a standard deviation:

$$\sigma_f(n) = \sqrt{\left(\frac{1}{2k}\right)\sum_{i=n-k}^{i=n+k}(f_p(i) - \overline{f_p(n)}\,)\text{^}2} \quad (10)$$

$$\overline{f_p(n)} = \left(\frac{1}{2k}\right)\sum_{i=n-k}^{n+k} f_p(i) \quad (11)$$

Where f_p represents the underlying parameter data resulting from the simulation. $2k$ denotes the rolling window over which the population is considered, and, as in the Gaussian filtering case, is taken to be 10 times the Gaussian standard deviation used. Performing simple averages and standard deviations of the raw CFD data seem to be heuristically sufficient. Each standard deviation set is then normalized by the Gaussian-filtered dataset, so that individual stability parameters are created. These are individually not definitive enough typically to yield an objective measure, but when the product of multiple parameters of interest is taken, the instabilities seem to be amplified such that an arbitrary yet objective value can be selected to definitively assess the position (and therefore mass flow rate) at which stall results in operation beyond the stability threshold. Thus, the amplified instability metric from the physical parameters becomes

$$I_p(n) = \prod_i \left(\frac{\sigma_{fp,i}(n)}{\bar{G}(f_{p,i})(n)}\right) \quad (12)$$

Note that this instability metric is very similar to the previous, with the addition that we use the rolling standard deviation function of a parameter rather than a parameter by itself.

3. RESULTS AND DISCUSSION

3.1 Four-Stage Centrifugal Blower

A four-stage centrifugal blower that was designed with the AxSTREAM™ platform was analyzed to evaluate its characteristic behavior. Of special interest was the location of instability with respect to stall and deep surge. Figure 11 and Figure 12 show the resulting characteristic speedline and instability metric. The flow and pressure ratio data has been normalized to the nominal design value to avoid disclosing proprietary data. The actual values are not pertinent to the present analysis. The mass flow rate is taken not from the outlet, where it is a specified boundary condition, but rather at the inlet, which enables the use of the parameter for both visualization and objective analytics.

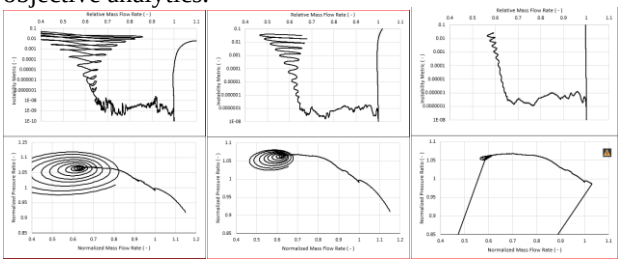

Figure 10: Qualitative view of effect of choice of σ = 10 (left), 30 (middle), and 50 (right)

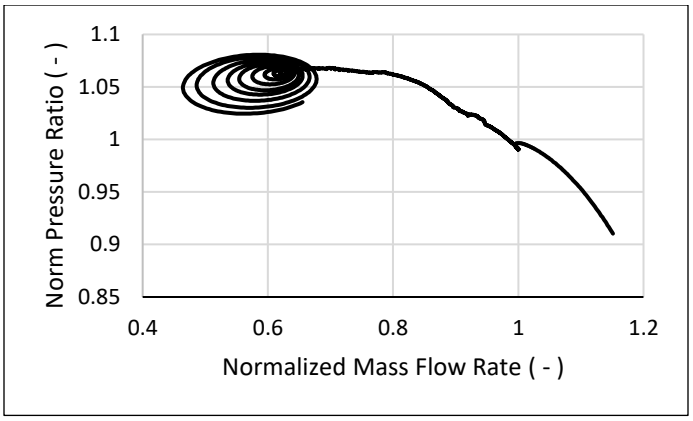

Figure 11: Centrifugal blower normalized characteristic curve with indication of instability

Both graphs of Figure 11 and Figure 12 were obtained by using the Gaussian filter. The number of samples used, as stated previously, spans 10 standard deviations of the Gaussian filter. The value of the standard deviation, σ, was heuristically tuned based on obtaining a visually sufficiently smooth characteristic and clear results on the instability metric. A value of $\sigma = 30$ seemed to give the most objective and satisfying results, however it should be noted that values from 10 to 50 were found to give the same objective value of deep surge and nearly the same speed line. This is qualitatively demonstrated in Figure 10, where values of σ of 10, 30, and 50 are shown with corresponding graphs. Although they are too small to extract quantitative results, they demonstrate the authors' visual indicators that were used to determine which value best filters the data set. As will be observed from the speed line characteristic, the maximum value of pressure ratio occurs at approximately 70% of nominal mass flow. Also clearly present in the speed line graph is the characteristic surge cycle at even lower mass flow rates, even though the data has been filtered and is continuously simulating at near steady-state conditions. It will be noticed that the term "surge" is used to describe what is being observed from the numerical experiments, even though it should be noted clearly that, strictly speaking, surge is a system phenomenon rather than just a flowpath phenomenon. The domain of the simulation only extends slightly upstream of the inlet guide vanes and includes the outlet of the volute – hardly a whole system. Nevertheless, even with the modest extension of the domain, the characteristic mass flow fluctuations are clearly evident, along with corresponding pressure fluctuations that make the classic surge cycle.

Turning attention to Figure 12 and the instability metric, it becomes apparent the usefulness of an objective characterization of instability. The metric used for this particular machine was based entirely on physical data. More specifically, the field functions were used to evaluate the (i) mass flow rate at the inlet, (ii) total-total isentropic efficiency, (iii) fluid power as measured by the total mass flow multiplied with the total enthalpy rise, and (iv) total-total pressure ratio at each iteration. The standard deviation filter of Equations (10) and (11) were applied, normalized by the Gaussian filter of Equation (7), to get an

arbitrary non-dimensional indicator of stability for each of the four physical parameters. The product of the physical instability parameters was then taken to amplify the result as per Equation (12) and this results in the overall physical instability metric. For the radial four stage blower, this was the only instability metric used and needed. To present the data, the Gaussian-filtered flow rate is used as the independent variable against which to plot the amplified instability metric. The result is Figure 12, where the instability metric is plotted on a logarithmic scale.

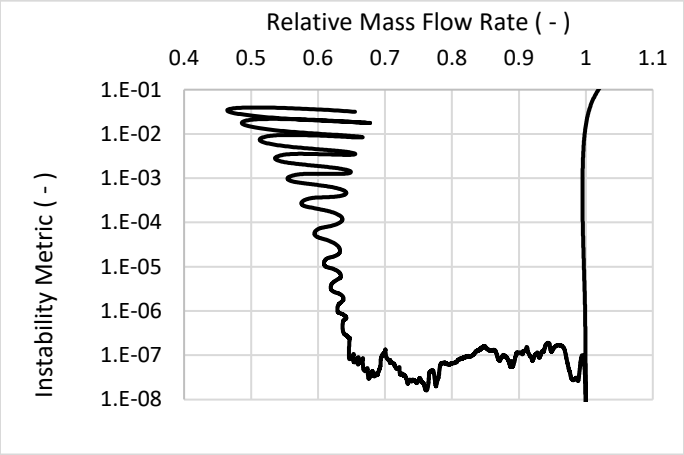

Figure 12: Radial blower instability metric as derived from physical parameter variability

It is noted that the actual values of the instability metric have no particular meaning in the context of this analysis, so that the relative changes values between different parts of the operating regime provide the insight. One need only visually scan the instability characteristic for a baseline, choose a threshold value, and extract an objective value of mass flow rate for which the instability characteristic exceeds or passes the threshold. From the figure, it is seen that a baseline value of 10^{-7} is a reasonable choice, and that a threshold values between 10^{-6} to 10^{-5} are good choices. The metric gives clear indication of variation, even though the mass flow rate is varied (rather than pressure) to achieve the pseudo-steady state method, which has relatively low sensitivity to other parameters near stall/surge.

Because the instability axis is logarithmic, and the amplification of instability, there is clear indication between where the solution is relatively stable between 0.63 to 1 relative mass flow rate, and where there is deep surge, as indicated by the fundamental instability. As hypothesized, although the peak pressure rise occurs at a mass flow rate of 0.7 of the nominal flow rate and even drops off slightly as flow is reduced, the machine can continue to operate stably between 0.63 and 0.7 as long as the system curve is sufficiently steep to prevent oscillations.

3.2 NASA Transonic 2-Stage Compressor

The method is next applied to NASA's open case of a 2-stage transonic compressor [12]. For this set of simulations, the ramp was performed with an exit static pressure boundary condition, starting from a nominally low value of 171kPa (or a total-to-static pressure ratio of 1.69) and slowly increasing. This was done because the range of operation of this particular design is relatively narrow, while the exact location of choke was not truly known. The nominal design parameters are listed in Table 3. The decision to use a pressure boundary condition undoubtedly has ramifications on the nature of the simulation as near-stall instability is approached. It will be seen, however, that the instability metric provides good results that is in agreement with literature reported values.

The resulting maximum speed line characteristic that shows the underlying CFD data and the Gaussian-filtered data is shown in Figure 13. The motivation for filtering the raw data is clear, especially near the peak pressure region where stall tends to onset and where it is seen that the instability results in significant fluctuations in flow rate. As in the previous study involving the radial blower, the filtering window and standard deviation for the Gaussian filter function was heuristically chosen to achieve a visually smooth curve. The value is $\sigma = 70$ with a corresponding window of $2k = 10\sigma = 700$. It must be pointed out that the filtered (blue) data does not quite rise to the same peak as the unfiltered (black) data, and this is the tradeoff of filtering, where a denser set of data exists toward the lower flow and lower pressure area and therefore has some influence on the curve. Figure 14 shows the CFD-derived speed line of this method (plotted by extracting discrete representative points from the filtered data) against the entire compressor map with the experimental speed lines for 70%, 80%, 90%, and 100% speed with AxSTREAM™ 1D analysis.

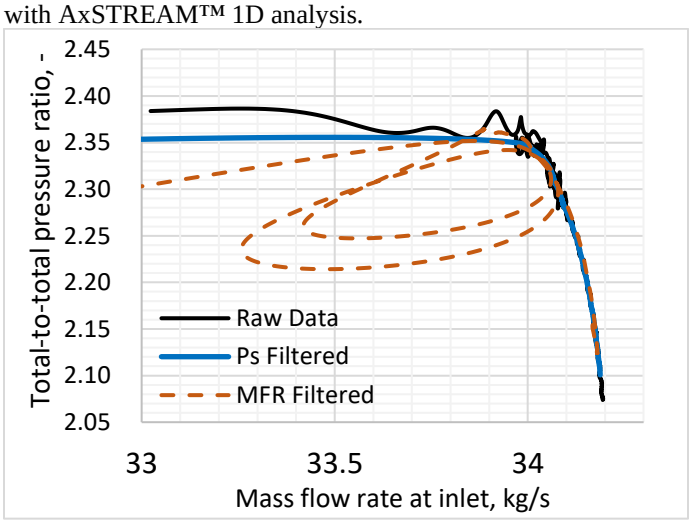

Figure 13: Characteristic speed line at maximum operating speed showing raw CFD results (black) with Gaussian-filtered results (blue) superimposed. Additional filtered data with a MFR boundary condition is shown (orange stripe)

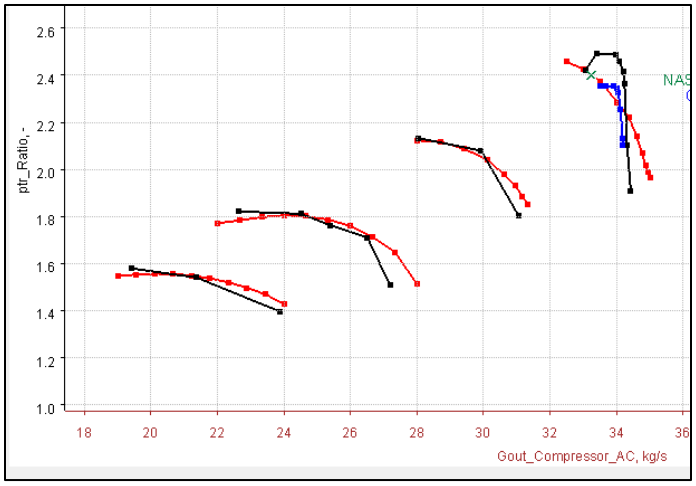

Figure 14: Compressor total pressure ratio map of subject 2-stage axial machine at speed ratios 1, 0.9, 0.8, and 0.7 comparing experimental (black), AxSTREAM 1D predictions (red), and CFD-derived characteristic (blue)

As is seen from the compressor map, the pseudo-steady state CFD method results in a very close match at the speed line of interest, with the choke line matching almost perfectly to experimental data. The largest error is in the prediction of peak total pressure ratio, which may be attributed to disparate specific locations of measurement between CFD and experiment (for example the CFD simulation domain has a generous extension), various experimental and manufacturing factors, and potentially modeling errors. However, it may already be apparent, and will be further confirmed by the analysis, that the mass flow rate at which stall occurs agrees very well with experiment. The value reported in the literature is 34.01 kg/s.

We will now individually review and evaluate the residual-based, imbalance-based, and physical parameter variation based instability metrics. All stability Gaussian filters reduced the value of $\sigma = 50$ to attain heuristically optimum objective characterization, although a significant variation in the value of σ could have been used with similar results. Starting with the evaluation of residuals, we use the formulation shown in Equation (8) to present the instability data. Here, the overall simulation domain normalized root-mean-square (RMS) values of the three momentum equations, mass-conservation, energy conservation, and two equation turbulence model are directly multiplied. The resulting metric is than transformed via the Gaussian filter and plotted against Gaussian-filtered flow rate.

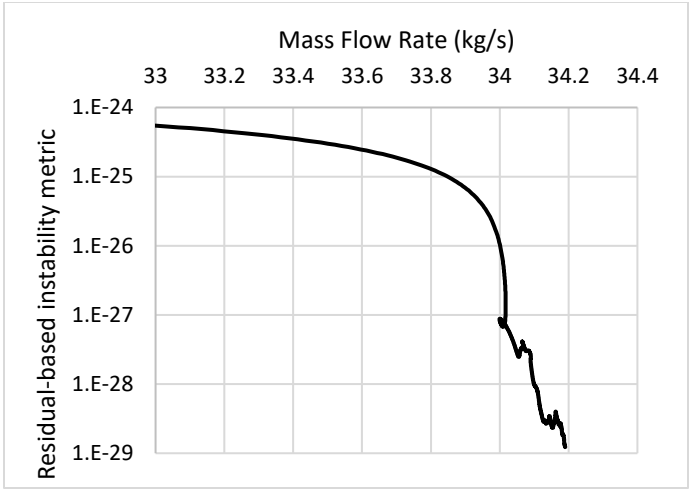

Figure 15: Residual-based instability metric using Gaussian-filter of the product of overall RMS residuals

It should be clear by examination of the processed data that an objective value of residual-based instability metric can be selected upon which the severe-stall mass flow rate could be determined. In this case, a value between 33.9kg/s and 34kg/s would likely be determined. However, the authors will note that RMS-residual rise may be associated with the method of using a pressure-based outlet boundary condition which becomes very sensitive near stall. The residual-based method did not yield a reliable indicator of instability for the previous radial blower. It will be noted that a subsequent simulation using outlet mass flow rate as the swept boundary condition resulted in a residual-based metric that was also not a reliable indicator of physical stability, confirming that the sensitivity of the simulation near stall to the pressure boundary is likely responsible for the definitive indication.

Next the indicators based on imbalances are generated. There are five imbalances reported – mass, energy, and three cartesian momentum. There are also four domains in the simulation, which are the two rotors and two stators. Therefore, a total of 20 values of physical imbalance are reported at each CFD iteration. For the purposes of methodological evaluation, the data postprocessing is done in two ways. The first is to perform Gaussian filtering on each individual imbalance, followed by taking the product of the resulting filtered values at each iteration, per the formula of Equation (9). The results of this are presented in Figure 16. Alternatively, a procedure similar to Equation (8) can be followed, where the product of the imbalances is first taken, and the result are then passed through the Gaussian filter. This is shown in Figure 17.

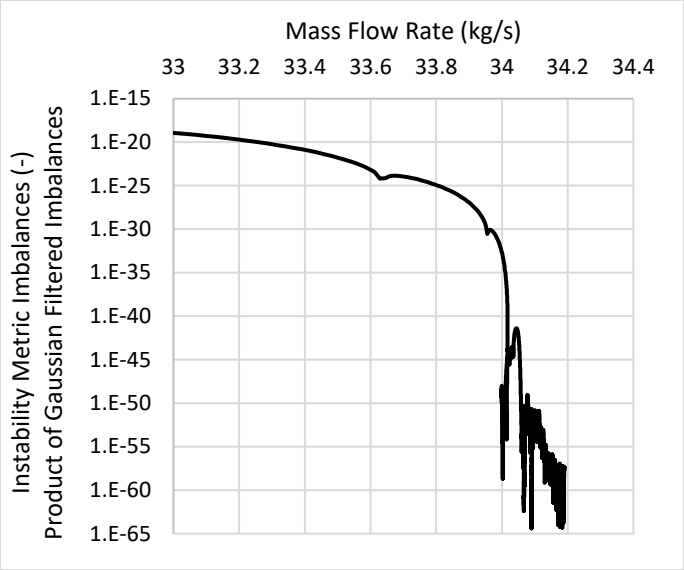

Figure 16: Instability metric using product of Gaussian-filtered imbalance data

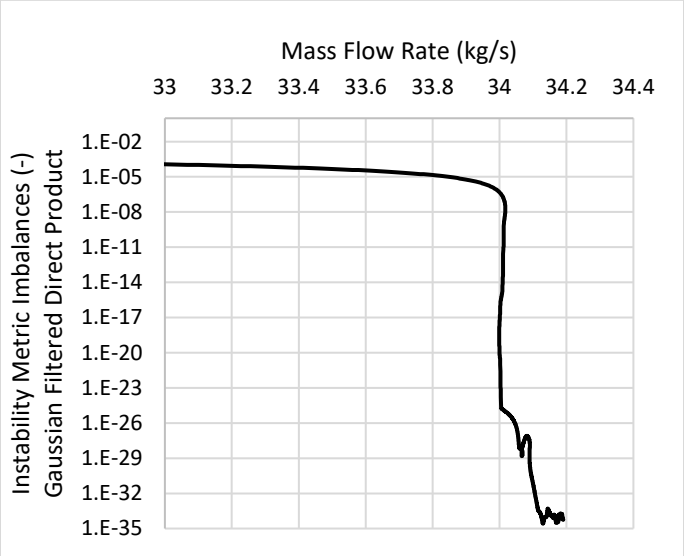

Figure 17: Instability metric using Gaussian-filter of the product of imbalances

The authors recommend the former approach as shown in Figure 16, even though the later one results in a more clearly defined rise in the resulting instability metric at the experimentally established stall mass flow rate. The justification, however, is that small numerical fluctuations in the imbalances may occur. These imbalances are numerical in the present case because the solver is attempting to generate the steady state solution, so fluctuations can be due to several factors such as relaxation factors and false timestep value and ideally are centered about zero if the simulation is near physical convergence and steady-state. Therefore, taking a filter first enables the averaging out the zero-centered fluctuations and amplifies the imbalances that may not be precisely centered about zero, which is objectively a stronger indication that something is unstable, or that even the simulation is invalid if the values are sufficiently high. The subsequent simulation of the NASA 2-stage compressor using an outlet MFR boundary condition resulted in an imbalance-based instability metric that was less clear-cut for the same sensitivity reasons as already discussed, although it led to similar conclusions.

Finally, the instability metric based on physical values is calculated by post-processing according to Equation (12), which is the same as the previous section. The physical values in this case include a multitude of mass-flow-averaged parameters at 5 stations in the flow path. At each of the stations, the total and static enthalpies, pressures, static entropies, as well as integral performance metrics that include mass flow rate, torque-based power consumption of each rotor row are reported. The results are shown in Figure 18.

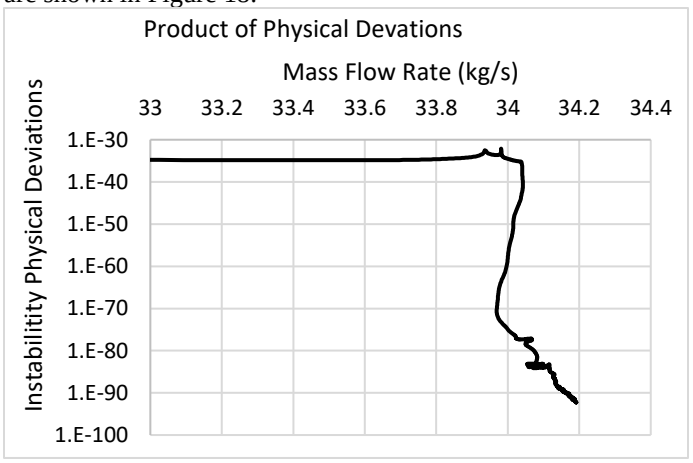

Figure 18: Instability metric using product of physical deviations

It should be clear that once a nominal baseline is selected within the normal operating range (say 34.0ks/s to 34.2kg/s), a reasonable threshold value that is a few orders of magnitude higher than the baseline will yield an answer within a tight range for where the deep instability occurs, which is between 33.95 and 34.05kg/s, agreeing with experiment very well.

We can take the product of all three classes of instability metrics to yield an overall metric that is conjectured to yield the "best of all worlds" in the sense of averaging the noise while amplifying different sources of instabilities. As discussed in the foregoing paragraphs, we deliberately select the imbalance metric of Figure 16 instead of the other one. Taking the product of the three instability metrics we obtain the results shown in Figure 19 and Figure 20, which zoom the data near the stable operating envelope and further out, respectively.

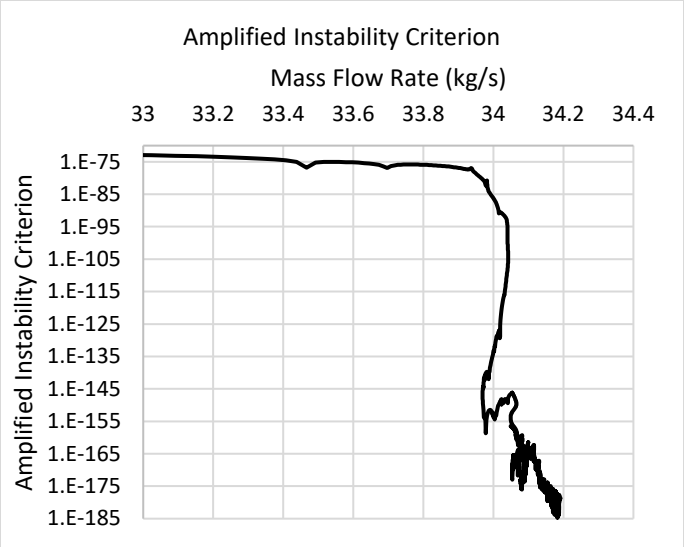

Figure 19: Amplified instability metric zoomed to stable operating regime

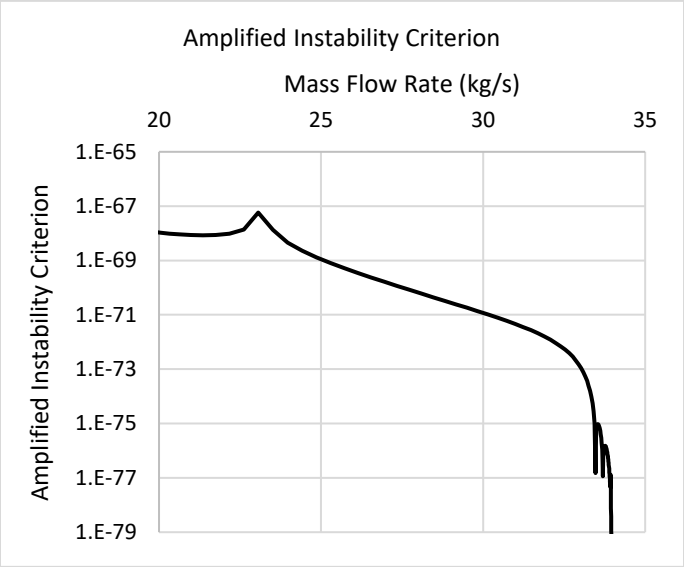

Figure 20: Amplified instability metric shown over expanded region

When first examining the zoomed-in instability metric, it becomes apparent that the baseline should exist somewhere below 1×10^{-145}. A reasonable value for a threshold would be in the range [1×10^{-145}, 1×10^{-85}] which results in the stall location to be predicted between 33.98kg/s and 34.04kg/s – a very close agreement to the 34.01kg/s attained by experiment.

Finally, looking at the zoomed out data, it is interesting to observe that the overall metric shows a continuing rise in instability as mass flow rate is decreased. It should be acknowledged that no firm conclusions can be drawn from the latter observation because the method of setting the boundary condition using pressures at both inlet and exit has a high sensitivity near the stall and lower mass flow rates and that relative shape of the overall instability metric may be different with a mass flow rate boundary condition. Nevertheless, the shape that is seen in the data is somewhat suggestive of the stability being a continuous nature. It can be conclusively stated that, upon a follow-up simulation using a mass-flow boundary at the outlet, that stable operation below a flow rate of 33kg/s, as may be suggested by Figure 20, is unlikely even with a steep system curve. However, even with the MFR boundary condition the simulation suggests that there is a relative stability zone between 33.9kg/s and 34.0kg/s where small flow/pressure oscillations can be expected but overall the machine can aerodynamically function. Of course, it is not suggested that designing a system curve to take advantage of such potential capability is not risky business.

3.3 Pump Cavitation

Finally, the method was applied to derive a cavitation characteristic to a subject pump. The use of such a method is documented in [13]. Traditionally, steady-state RANS CFD can be used at specific operating points to draw a locus of points. In this study, the sweep across the suction pressure of the pump was numerically performed in CFD until the simulation shows a drastic drop in total pressure rise of the pump.

Although it may be interesting in a future study to perform stability analysis of the results, it was deemed unnecessary for the purposes set forth. The unfiltered results are sufficiently smooth, as shown in Figure 21.

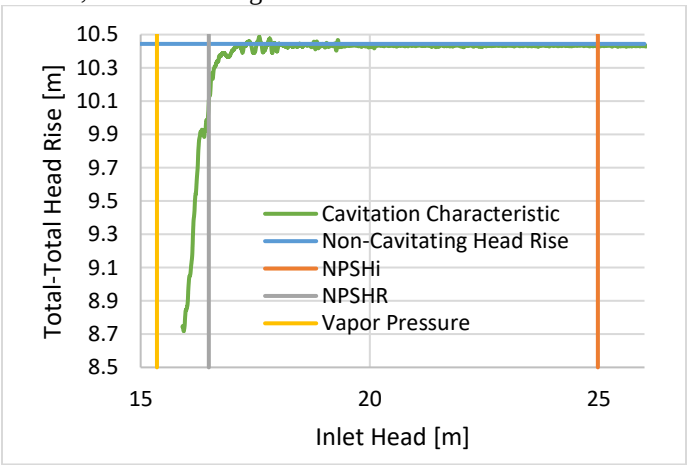

Figure 21: Pump cavitation characteristic derived using pseudo-steady state approach method with no filtering applied

It quite clear that the $NPSH_R$ value (or required net positive suction head to avoid a 3% drop in pressure rise) can be extracted objectively and is shown by the gray vertical line. Furthermore, some fluctuations in the data are seen in the cavitating region where bubble collapse is likely to cause damage, indicating that there may be a correspondence between underlying physical phenomena of cavitation and the stability of the solution from one iteration to the next.

4. CONCLUSION

In this paper, a methodology for generating a near continuous performance curve of a turbomachine over a range of

operation that uses steady-state RANS CFD methods to effectively sweep across an operating characteristic in a pseudo-steady state way was shown. The operating characteristic may be, but need not necessarily be, a speed line. Further, methodology to post-process the CFD data that not only reveals a smooth operating characteristic, but information about the operating stability of the machine that is extremely useful for the determination of limits of operation, especially stall, is also described.

Three test cases have also been presented where the method was used to find important operating characteristics of interest. The cases presented were an industrial multistage radial air blower that was in the design phase, a two-stage aero engine fan-compressor that was used as a validation case, and finally a conceptual pump for which a cavitation characteristic needed to be evaluated.

It was shown that the method was able to generate a performance curve for all machines. Furthermore, the method was able to determine that deep stall – where instability causes large fluctuations in flow and pressure rise – occurs further to the left of the peak pressure rise on the pressure-flow speed line for the case of the radial multistage blower, as was hypothesized. This is an important result that has ramifications on overall machine design considerations.

It is also noted that the method described, while not directly suited for detailed flow field analysis, allows for practical engineering characterization of machines using CFD with less or equal computational time and engineering effort than typically required to execute analyses of individual points. It is recognized that exact wall-clock time is not explicitly tracked and compared against typical discrete operating point analyses. It would indeed be of interest in a future study to perform this measurement for a typical simple case where results could be repeated with reasonable expenditures of computational resources.

Finally, it should be noted, perhaps as motivation for future research, that the method of post-processing iteration data using a Gaussian filter has potential application to analyzing transient CFD analysis data. Transient analyses were not within the scope of the present research, however, the potential to gain significant additional insight is recognized. A particular challenge is that the integral parameters of interest (such as flow, pressure ratio, power, etc.) also have temporal fluctuations, whereas the focus of the results is to obtain overall/integral steady-state performance predictions. Thus, the filtering methodology described herein is also potentially suited to transient methods.

ACKNOWLEDGEMENTS

The authors would like to thank SoftInWay, Inc. for sponsoring this work and allowing its publication.

REFERENCES

[1] Roberts, Douglas A., and Robin Steed. "A comparison of steady-state centrifugal stage CFD analysis to experimental rig data." In *Submitted to the 2004 ANSYS CFX conference*. 2004.

[2] Dixon, Sydney Lawrence, and Cesare Hall. *Fluid mechanics and thermodynamics of turbomachinery*. Butterworth-Heinemann, 2013.

[3] Cumpsty, Nicholas A. "Compressor aerodynamics." *Longman Scientific & Technical* (1989).

[4] Ronald, H. "Centrifugal compressors: A strategy for aerodynamic design and analysis." *American Society of Mechanical Engineers Press* (2000).

[5] Hipple, Samuel M., Harry Bonilla-Alvarado, Paolo Pezzini, Lawrence Shadle, and Kenneth M. Bryden. "Using machine learning tools to predict compressor stall." *Journal of Energy Resources Technology* 142, no. 7 (2020): 070915.

[6] Righi, Mauro, Vassilios Pachidis, László Könözsy, and Lucas Pawsey. "Three-dimensional through-flow modelling of axial flow compressor rotating stall and surge." *Aerospace Science and Technology* 78 (2018): 271-279.

[7] Vagani, Marco, Abraham Engeda, and Michael J. Cave. "Prediction of impeller rotating stall onset using numerical simulations of a centrifugal compressor. Part 1: Detection of rotating stall using fixed-flow transient simulations." *Proceedings of the Institution of Mechanical Engineers, Part A: Journal of Power and Energy* 227, no. 4 (2013): 403-414.

[8] Munari, Enrico, Gianluca D'Elia, Mirko Morini, Emiliano Mucchi, Michele Pinelli, and Pier Ruggero Spina. "Experimental investigation of vibrational and acoustic phenomena for detecting the stall and surge of a multistage compressor." *Journal of Engineering for Gas Turbines and Power* 140, no. 9 (2018).

[9] Schiavello, Bruno, and Frank C. Visser. "Pump Cavitation: various NPSHR criteria, NPSHA margins, impeller life expectancy." In *Proceedings of the 25th international pump users symposium*. Texas A&M University. Turbomachinery Laboratories, 2009.

[10] Menter, Florian R. "Two-equation eddy-viscosity turbulence models for engineering applications." *AIAA journal* 32, no. 8 (1994): 1598-1605.

[11] Sparrow, Ephraim M., John M. Gorman, John P. Abraham, and Wally Minkowycz. "Validation of turbulence models for numerical simulation of fluid flow and convective heat transfer." In *Advances in Heat Transfer*, vol. 49, pp. 1-35. Elsevier, 2017.

[12] C. L. Ball, L. Reid and J. F. Schmidt, "End-Wall Boundary Layer Measurements in a Two-Stage Fan (NASA-TM-83409)," NASA, 1983.

[13] Goldenberg, Vlad, Andrey Sherbina, Evgen Rublevskiy, Ben Conser, and Tishun Zhang. "Cavitation Prediction and Avoidance in Design using Semi." In *Proceedings of the 37th International Pump Users Symposium*. Turbomachinery Laboratory, Texas A&M Engineering Experiment Station, 2021

